ChemComm

COMMUNICATION

View Article Online
View Journal | View Issue

Cite this: *Chem. Commun.*, 2022, **58**, 12839

Received 22nd August 2022,
Accepted 30th September 2022

DOI: 10.1039/d2cc04647d

rsc.li/chemcomm

Structural region essential for amyloid fibril formation in cytochrome *c* elucidated by optical trapping†

Shun Hirota, *[a] Chun-Liang Chiu,[b] Chieh-Ju Chang,[b] Pei-Hua Lo,[b] Tien Chen, [b] Hongxu Yang,[a] Masaru Yamanaka,[a] Tsuyoshi Mashima, [a] Cheng Xie, [a] Hiroshi Masuhara [b] and Teruki Sugiyama *[ab]

Amyloid fibril formation of cytochrome *c* is spatially and temporally controlled with a combined method of disulfide bond cross-linking of cysteine-introduced variants and optical trapping, identifying that the structural change in the region containing Ala83 is essential for the amyloid fibril formation.

Proteins often function by forming specific three-dimensional structures, but they are structurally denatured and accumulate as amyloid fibrils in living tissues for the case of several diseases, including Alzheimer's disease, spongiform encephalopathies, and type II diabetes.[1] X-ray diffraction analysis revealed the fibrils to be ordered in the β-pleated sheet conformation, with the direction of the polypeptide backbone perpendicular to the fibril axis (cross-β structure).[2] Amyloid fibrils are recognized as long, nonbranched filaments with diameters of approximately 10 nm according to electron microscopy.[1c,2] Amyloid fibrils are often formed under high protein concentrations and preceded the formation of metastable, nonfibrillar species that contain an extensive β-sheet structure and can bind thioflavin T (ThT).[1a–c,3] However, spatially and temporally controlling the formation of amyloid fibrils is difficult, making it challenging to identify the key structural regions for amyloid fibril formation.

Cytochrome *c* (cyt *c*) is a well-known globular heme protein that transfers electrons from the cytochrome bc_1 complex to cytochrome *c* oxidase in the respiratory chain in mitochondria, whereas several new functions have been reported, such as a key role in apoptosis, cytosolic redox sensing and involvement in the mitochondrial oxidative folding machinery.[4] The heme of cyt *c* forms covalent bonds with two cysteine residues through their sulfur atoms, and His18 and Met80 are coordinated to the heme iron.[5] The folding character of cyt *c* has been thoroughly studied from the viewpoint of heme coordination[6] and protein folding units.[7] Cyt *c* is composed of five cooperative folding units, called foldons, and the reversible equilibrium unfolding of cyt *c* steps up through intermediate forms to the unfolded state in an energy-ordered sequence, one foldon unit at a time, in the order of the grey, red, yellow, green and blue structural regions shown in Fig. 1.[7] Cyt *c* forms amyloid fibrils when heated at 75 °C for 12 h under mild alkaline conditions[8] or when incubated overnight in the presence of anionic phospholipids.[9]

In 1986, optical trapping, also known as optical tweezers, with a single focused laser beam was first demonstrated by Ashkin *et al.*[10] The gradient force exerted on the target is given as a function of the electric field, magnetic flux density, and polarizability of the target and medium. Under focused laser irradiation, molecular diffusion in solution is slightly suppressed at the laser focus, where an optical potential well is

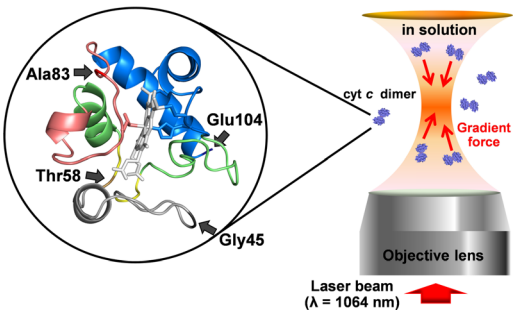

Fig. 1 Schematic view of the experiment. Left: Structure of horse cyt *c*. Five foldons are shown in blue, green, yellow, red and grey. The positions of mutated amino acid residues (Gly45, Thr58, Ala83 and Glu104) are shown in dark colours. The heme and the side chains of Cys14, Cys17, His18 and Met80 are shown in stick models. Right: Optical trapping method.

[a] *Division of Materials Science, Graduate School of Science and Technology, Nara Institute of Science and Technology, 8916-5 Takayama, Ikoma, Nara 630-0192, Japan. E-mail: hirota@ms.naist.jp*

[b] *Department of Applied Chemistry and Center for Emergent Functional Matter Science, National Yang Ming Chiao Tung University, 1001 University Road, Hsinchu 300093, Taiwan. E-mail: sugiyama@nycu.edu.tw*

† Electronic supplementary information (ESI) available. See DOI: https://doi.org/10.1039/d2cc04647d

generated.[11] The optical potential efficiently traps the second molecule, forming a transient aggregate through mutual association. With a larger volume of the formed aggregate, the potential becomes deeper, and by repeating this process, molecules can be highly concentrated at the laser focus.[12] In 2009, Tsuboi *et al.* demonstrated optical trapping of some proteins, lysozymes, cyt *c* and myoglobin to form microparticles.[13] Previously, we successfully obtained amyloid fibrils of cyt *c* by optical trapping of its domain-swapped dimers[14] despite the low amyloidogenicity of cyt *c*.[15] In fact, the domain swapping mechanism has been proposed as a mechanism to form amyloid fibrils.[16] Although cyt *c* is not a neurodegenerative disease protein, the well-studied folding character makes cyt *c* an affordable protein for investigating the nature of amyloid fibril formation with this optical trapping method. In this study, we revealed the structural region essential for amyloid fibril formation of cyt *c* by optical trapping of disulfide-linked dimers (Fig. 1).

To elucidate the structural region important for the amyloid fibril formation of cyt *c*, dimers with an intermolecular disulfide bond at various positions (Gly45, Thr58, Ala83 and Glu104) in different foldons were used to restrict the structural flexibility of different regions during optical trapping (Fig. 1). According to circular dichroism measurements, the monomers and disulfide-linked dimers of cyt *c* variants showed secondary structures similar to those of the wild-type monomer; the spectra exhibited two negative bands at 208 and 222 nm, which represent the α-helical structure (Fig. S1, ESI†). These results indicate that the disulfide bond did not significantly alter the secondary structures of cyt *c*, whereas domain swapping slightly perturbed the secondary structures of cyt *c*.

A linearly polarized continuous-wave laser (300 mW) with a wavelength of 1064 nm was focused with an objective lens in a D_2O solution for optical trapping experiments (Fig. S2, ESI†). The laser power density (18 MW cm^{-2}; laser power: 0.3 W; irradiation area: 1.6×10^{-8} cm^2) was too low to cleave disulfide bonds *via* three-photon absorption. When optical trapping was applied to the solutions containing disulfide cross-linked dimers of the G45C, T58C and E104C cyt *c* variants, aggregates with a diameter of 4 ± 0.2 μm, which were estimated from the transmission images, were initially formed at the focal point according to microscopic observation (Fig. 2b and Fig. S3b and S4b, ESI†). The aggregate size of 4 μm was slightly larger than the spot size of 1 μm. Such a phenomenon has been frequently observed in the optical trapping of large molecules such as polymers and proteins, which is ascribed to intermolecular interactions, heat transfer and solvent flow.[12] This is phenomenologically similar to that of optical trapping of domain-swapped wild-type cyt *c* dimers.[14] When the aggregates of the G45C, T58C and E104C variants were continuously irradiated with a laser beam, the transmittance of the aggregate center in the CCD image gradually decreased, while the size was almost constant (Fig. 2c and Fig. S3c and S4c, ESI†). This indicates that the density of the variants within the aggregates increased through their optical trapping. Indeed, the density increase enhances the gradient force exerted on the aggregate, which brings the CCD image into sharp focus, as shown in Fig. 2c–e, as

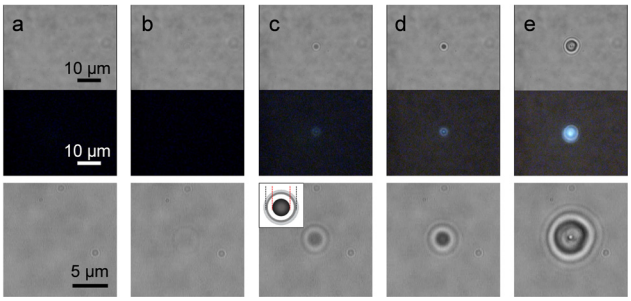

Fig. 2 Time-lapse transmission (top and bottom) and fluorescence (middle) images observed during the optical trapping of the G45C cyt *c* dimer at a laser power of 300 mW: (a) before optical trapping and after optical trapping for (b) 24 min, (c) 43 min, (d) 48 min and (e) 58 min. The aggregation dynamics can also be seen in Movie S1 (ESI†). The fluorescence images were captured at the same place where the movie in black was recorded. The upper left figure in the third row of Fig. 2c represents a schematic diagram of the generated aggregate of the CCD image, in which the black and red dotted lines are the standards for estimating the sizes of the aggregate and center core, respectively.

the laser focus coincides with the center of a sphere of the aggregate. Upon further irradiation with the laser beam, the transmittance of the aggregate center in the CCD image remarkably decreased in a relatively short time, and its size reduced by apparently 0.2 μm in diameter (Fig. 2d and Fig. S3d and S4d, ESI†). The slight decrease in the aggregate size suggests that the variants within the aggregates were densely packed by optical trapping. Along with the size decrease, the fluorescence intensity of ThT coexisting in the solution significantly increased, suggesting the formation of amyloid fibrils (Fig. 2d and Fig. S3d and S4d, ESI†). Subsequently, with continuous laser irradiation, the aggregate exhibited strong fluorescence from ThT and rapidly became larger, indicating that elongation of amyloid fibrils occurred at high speed (Fig. 2e and Fig. S3e and S4e, ESI†). The aggregate continuously grew with the laser irradiation and was suddenly expelled from the focal point. This occurred because the scattering force proportional to the sixth power of the target size overcame the gradient force proportional to its third power. The formation of an aggregate with a diameter of several μm was also observed when the 1064-nm laser beam was focused on the disulfide-linked dimer of the A83C variant, but no significant nonlinear increase in the ThT fluorescence intensity was detected (Fig. S5, ESI†).

After aggregates of the G45C, T58C and E104C cyt *c* variants were prepared on glass substrates, each aggregate was unwound by sonication and subjected to transmission electron microscopy (TEM) observation (Fig. 3). The features of the fibrils were all similar to those produced by optical trapping of the wild-type cyt *c* domain-swapped dimer: widths of 5–10 nm.[14] These results show that the G45C, T58C and E104C variants form amyloid fibrils by optical trapping of disulfide-linked dimers similar to the wild-type cyt *c* domain-swapped dimer, supporting the hypothesis that the structural flexibility around Gly45, Thr58 and Glu104 is not essential for amyloid fibril formation in cyt *c*.

The temporal changes in the size of the aggregate and the fluorescence intensity at 493 nm of the coexisting ThT at the

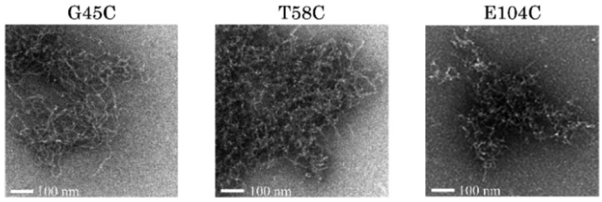

Fig. 3 Transmission electron microscopy images of amyloid fibrils obtained by optical trapping of the dimers of cyt *c* variants: G45C, T58C and E104C.

focal point showed three phases during optical trapping of disulfide-linked dimers of the G45C, T58C and E104C cyt *c* variants, leading to the formation of amyloid fibrils (Fig. 4 shows a typical case). In the initial phase A, the concentration of cyt *c* dimers increased in the focal volume, forming an aggregate approximately 4 μm in diameter. With further irradiation, the transmission at the center of the aggregate gradually decreased with the increase in the local concentration at the center due to the optical trapping of the cyt *c* dimer molecules. In the second phase B, decreases in the transmission and apparent aggregate size at the center and an increase in the fluorescence intensity were observed in a relatively short period, indicating a change in the aggregate state. This phase may correspond to a structural change from the native structure to a protofibril, which can bind ThT.[3b,17] Subsequently, the size of the aggregate and the ThT fluorescence intensity rapidly increased (phase C), indicating rapid amyloid fibril elongation. Concerning the heme structure of cyt *c* during optical trapping, the resonance Raman spectra before and after amyloid fibril formation were similar to the spectrum of ferric cyt *c* (Fig. S6, ESI†).[18] The ν_4 Raman band was observed at 1373 cm^{-1}, a typical frequency for the ferric state.[19] The intensity of the 1586 cm^{-1} ν_2 band corresponding to the low-spin six-coordinate ferric state slightly decreased due to amyloid fibril formation, whereas that of the 1566 cm^{-1} band corresponding to the high-spin ferric state slightly increased. These results indicate that the heme in cyt *c* was in the ferric state during the amyloid fibril transition, although the heme coordination structure may have slightly changed.

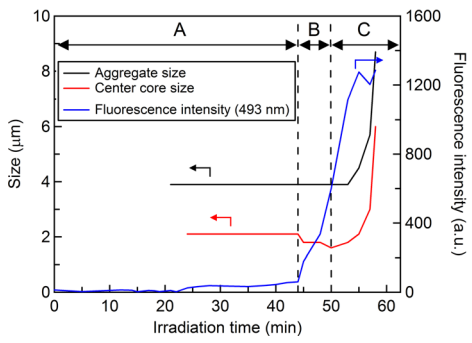

Fig. 4 Typical diagram of three phases (A–C) in terms of the aggregate size (black), center core size (red) and ThT fluorescence intensity at 493 nm (blue) induced by optical trapping of the disulfide-linked G45C cyt *c* dimer coexisting with ThT in solution.

The average times for phases A and B observed in optical trapping of the domain-swapped dimer of wild-type cyt *c* and disulfide-linked dimers of the G45C, T58C and E104C variants (Fig. 4 and Fig. S3f and S4f, ESI†) are listed in Table 1. The sizes of the cyt *c* dimers would not significantly differ judging from the structures of the monomer and domain-swapped dimer,[5,20] leading to similar trapping efficiency and aggregation behaviours for the dimers in phase A. High concentrations of proteins are reported to be necessary for amyloid fibril formation.[1b,c] The concentration of the cyt *c* dimers gradually increased at the laser focus in phase A, the period of which may correspond to the time to reach the high protein concentration necessary for the structural change. In phase B, the size of the aggregate decreased and the ThT fluorescence intensity was nonlinearly enhanced. The period of phase B may correspond to the time necessary for the protein to accomplish the structural change from the native structure to a protofibril. Thus, the periods of phases A and B correlate, both corresponding to the ability and flexibility of the region essential for amyloid fibril formation. In phase C, the fluorescence intensity of the coexisting ThT rapidly increased, strongly indicating elongation of the amyloid fibril from the protofibril.

Cyt *c* unfolds in the order of an Ω loop (residues 40–57), an Ω loop (residues 71–87), the neck of an Ω loop (residues 37–39 and 58–60), the 20's–30's Ω loop and 60's helix (residues 20–36 and 61–70), and N- and C-terminal helices (residues 1–19 and 88–104) (Fig. 1).[7] Cyt *c* formed amyloid fibrils for the variants linked with a disulfide bond through Cys residues introduced into various regions, except for the A83C variant. The time required to form aggregates (phase A) increased in the order of T58C < G45C < E104C (Table 1), whereas the time necessary for the apparent protein structural change (phase B) increased in the same order. Even though Gly45 is located in the foldon that unfolds first during cyt *c* unfolding,[7] amyloid fibrils formed faster in the optical trapping of the G45C cyt *c* dimer compared to the E104C cyt *c* dimer. These results show that the restriction of amyloid fibril formation for a disulfide-linked cyt *c* variant dimer is not related to the unfolding order of the foldon that contains the introduced Cys. Additionally, the times for phases A and B of the wild-type cyt *c* domain-swapped dimer were shorter than the corresponding times of other disulfide-linked dimers, indicating that the domain-swapped structure accelerates the amyloid fibril formation.

ThT coexisting in the solution did not show a substantial fluorescence enhancement for the optical trapping of the A83C

Table 1 Average times for phases A and B observed in optical trapping of the dimers of cyt *c* variants

	Type of dimer	Phase A (min)	Phase B (min)
Wild type	Domain-swapped	11 ± 3	1.0 ± 0.4
G45C	Disulfide-linked	34 ± 10	7.6 ± 2
T58C	Disulfide-linked	24 ± 5	2.4 ± 1
A83C	Disulfide-linked	—[a]	—[a]
E104C	Disulfide-linked	45 ± 7	15 ± 6

[a] No apparent fluorescence increase was observed.

cyt *c* dimer (Fig. S5, ESI†). The V83G mutation in human cyt *c* does not significantly alter the peroxidase activity, indicating little effect on the coordination structure of the mutation at the 83rd amino acid.[21] The loop structure in the Ile75–Lys87 region in a yeast iso-1 cyt *c* variant has been shown to change to a β-hairpin structure.[22] This region includes the hinge region (Lys79–Ala83) of domain swapping.[20] In our present study, the A83C variant forms a disulfide bond between Cys83 in the dimer, thereby limiting the structural flexibility around Cys83, which is located in the Pro71–Lys87 Ω loop, and inhibiting amyloid fibril formation. The Pro71–Lys87 Ω loop has been shown to change its conformation by cleavage of the heme-Met80 coordination bond.[23] Thr58 is on the edge of the protein and relatively far from Ala83 (25.4 Å between the α-carbons); thus, the structural change in the Ile75–Lys87 region may be less affected by disulfide bond formation at Thr58, resulting in the periods for phases A and B of the T58C cyt *c* dimer being the shortest among the cyt *c* variant dimers studied. These results strongly suggest that the structural change of the Ile75–Lys87 region from a loop to a β-hairpin is essential for amyloid fibril formation in cyt *c*.

In conclusion, we investigated the amyloid fibril formation of cyt *c* by spatially and temporarily controlling the aggregation *via* optical trapping of disulfide-linked dimers of various Cys-introduced variants, where the time required to form aggregates increased in the order of T58C < G45C < E104C. Additionally, no apparent amyloid fibril formation was detected in optical trapping of the disulfide dimer of the A83C cyt *c* variant under the same conditions. The differences in the ability of the variants to form amyloid fibrils did not depend on the folding region (foldon) to which the introduced Cys belonged; instead, they are attributed to the flexibility of the protein region around the introduced Cys. Three-dimensional amyloid fibril structures for peptides have been elucidated by X-ray crystallography,[24] but the amyloid structures are usually unobtainable for proteins, presumably due to the fluctuation of the nonamyloid fibrillation region. Our study elucidates that the region containing Ala83, presumably the Ile75–Lys87 Ω loop, is essential for amyloid fibril formation in cyt *c*. These findings not only elucidate the region essential for the structural change in the amyloid fibril formation of cyt *c* but also provide a new way to use optical trapping for studying biological events related to protein structural changes.

We thank Mr Masahiro Fujihara and Ms Tomoko Ohno, Nara Institute of Science and Technology, for their help in TEM measurements.

Conflicts of interest

There are no conflicts to declare.

Notes and references

1 (*a*) J. D. Sipe and A. S. Cohen, *J. Struct. Biol.*, 2000, **130**, 88–98; (*b*) F. Chiti and C. M. Dobson, *Annu. Rev. Biochem.*, 2006, **75**, 333–366; (*c*) J. Greenwald and R. Riek, *Structure*, 2010, **18**, 1244–1260; (*d*) P. H. Nguyen, A. Ramamoorthy, B. R. Sahoo, J. Zheng, P. Faller, J. E. Straub, L. Dominguez, J. E. Shea, N. V. Dokholyan, A. De Simone, B. Ma, R. Nussinov, S. Najafi, S. T. Ngo, A. Loquet, M. Chiricotto, P. Ganguly, J. McCarty, M. S. Li, C. Hall, Y. Wang, Y. Miller, S. Melchionna, B. Habenstein, S. Timr, J. Chen, B. Hnath, B. Strodel, R. Kayed, S. Lesne, G. Wei, F. Sterpone, A. J. Doig and P. Derreumaux, *Chem. Rev.*, 2021, **121**, 2545–2647; (*e*) M. I. Ivanova, Y. Lin, Y. H. Lee, J. Zheng and A. Ramamoorthy, *Biophys. Chem.*, 2021, **269**, 106507.
2 M. Sunde and C. Blake, *Adv. Protein Chem.*, 1997, **50**, 123–159.
3 (*a*) R. N. Rambaran and L. C. Serpell, *Prion*, 2008, **2**, 112–117; (*b*) D. M. Walsh, D. M. Hartley, Y. Kusumoto, Y. Fezoui, M. M. Condron, A. Lomakin, G. B. Benedek, D. J. Selkoe and D. B. Teplow, *J. Biol. Chem.*, 1999, **274**, 25945–25952; (*c*) J. Adamcik and R. Mezzenga, *Angew. Chem., Int. Ed.*, 2018, **57**, 8370–8382; (*d*) D. Willbold, B. Strodel, G. F. Schroder, W. Hoyer and H. Heise, *Chem. Rev.*, 2021, **121**, 8285–8307.
4 (*a*) Y. P. Ow, D. R. Green, Z. Hao and T. W. Mak, *Nat. Rev. Mol. Cell Biol.*, 2008, **9**, 532–542; (*b*) D. Alvarez-Paggi, L. Hannibal, M. A. Castro, S. Oviedo-Rouco, V. Demicheli, V. Tortora, F. Tomasina, R. Radi and D. H. Murgida, *Chem. Rev.*, 2017, **117**, 13382–13460; (*c*) S. Hirota and S. Nagao, *Bull. Chem. Soc. Jpn.*, 2021, **94**, 170–182.
5 (*a*) R. E. Dickerson, T. Takano, D. Eisenberg, O. B. Kallai, L. Samson, A. Cooper and E. Margoliash, *J. Biol. Chem.*, 1971, **246**, 1511–1535; (*b*) G. W. Bushnell, G. V. Louie and G. D. Brayer, *J. Mol. Biol.*, 1990, **214**, 585–595.
6 S. R. Yeh, S. W. Han and D. L. Rousseau, *Acc. Chem. Res.*, 1998, **31**, 727–736.
7 (*a*) Y. Bai, T. R. Sosnick, L. Mayne and S. W. Englander, *Science*, 1995, **269**, 192–197; (*b*) W. Hu, Z. Y. Kan, L. Mayne and S. W. Englander, *Proc. Natl. Acad. Sci. U. S. A.*, 2016, **113**, 3809–3814.
8 N. S. de Groot and S. Ventura, *Spectroscopy*, 2005, **19**, 199–205.
9 J. M. Alakoskela, A. Jutila, A. C. Simonsen, J. Pirneskoski, S. Pyhajoki, R. Turunen, S. Marttila, O. G. Mouritsen, E. Goormaghtigh and P. K. J. Kinnunen, *Biochemistry*, 2006, **45**, 13447–13453.
10 A. Ashkin, J. M. Dziedzic, J. E. Bjorkholm and S. Chu, *Opt. Lett.*, 1986, **11**, 288.
11 M. A. Osborne, S. Balasubramanian, W. S. Furey and D. Klenerman, *J. Phys. Chem. B*, 1998, **102**, 3160–3167.
12 T. Sugiyama, K. Yuyama and H. Masuhara, *Acc. Chem. Res.*, 2012, **45**, 1946–1954.
13 Y. Tsuboi, T. Shoji, M. Nishino, S. Masuda, K. Ishimori and N. Kitamura, *Appl. Surf. Sci.*, 2009, **255**, 9906–9908.
14 K. I. Yuyama, M. Ueda, S. Nagao, S. Hirota, T. Sugiyama and H. Masuhara, *Angew. Chem., Int. Ed.*, 2017, **56**, 6739–6743.
15 Y. Lin, J. Kardos, M. Imai, T. Ikenoue, M. Kinoshita, T. Sugiki, K. Ishimori, Y. Goto and Y. H. Lee, *Langmuir*, 2016, **32**, 2010–2022.
16 (*a*) M. J. Bennett, M. R. Sawaya and D. Eisenberg, *Structure*, 2006, **14**, 811–824; (*b*) E. Zerovnik, V. Stoka, A. Mirtic, G. Guncar, J. Grdadolnik, R. A. Staniforth, D. Turk and V. Turk, *FEBS J.*, 2011, **278**, 2263–2282.
17 J. D. Harper, C. M. Lieber and P. T. Lansbury, Jr., *Chem. Biol.*, 1997, **4**, 951–959.
18 M. Okada, N. I. Smith, A. F. Palonpon, H. Endo, S. Kawata, M. Sodeoka and K. Fujita, *Proc. Natl. Acad. Sci. U. S. A.*, 2012, **109**, 28–32.
19 (*a*) T. Jordan, J. C. Eads and T. G. Spiro, *Protein Sci.*, 1995, **4**, 716–728; (*b*) T. Kitagawa and S. Hirota, in *Handbook of Vibrational Spectroscopy*, ed. J. M. Chalmers and P. R. Griffiths, John Wiley & Sons Ltd., Chichester, 2002, vol. 5, pp. 3426–3446.
20 (*a*) S. Hirota, Y. Hattori, S. Nagao, M. Taketa, H. Komori, H. Kamikubo, Z. Wang, I. Takahashi, S. Negi, Y. Sugiura, M. Kataoka and Y. Higuchi, *Proc. Natl. Acad. Sci. U. S. A.*, 2010, **107**, 12854–12859; (*b*) S. Hirota, T. Mashima and N. Kobayashi, *Chem. Commun.*, 2021, **57**, 12074–12086.
21 H. Lei, S. M. Nold, L. J. Motta and B. E. Bowler, *Biochemistry*, 2019, **58**, 2921–2933.
22 J. F. Amacher, F. Zhong, G. P. Lisi, M. Q. Zhu, S. L. Alden, K. R. Hoke, D. R. Madden and E. V. Pletneva, *J. Am. Chem. Soc.*, 2015, **137**, 8435–8449.
23 L. J. McClelland, T. C. Mou, M. E. Jeakins-Cooley, S. R. Sprang and B. E. Bowler, *Proc. Natl. Acad. Sci. U. S. A.*, 2014, **111**, 6648–6653.
24 R. Riek and D. S. Eisenberg, *Nature*, 2016, **539**, 227–235.

